Programmed iron oxide nanoparticles disintegration in anaerobic digesters boosts biogas production.

Eudald Casals, Raquel Barrena, Ana García, Edgar González, Lucía Delgado, Xavier Font,

Jordi Arbiol, Pieter Glatzel, Kristina Kvashnina, Antoni Sánchez, and Víctor Puntes*

(*)   Prof. V. Puntes, E. Casals
 Institut Català de Nanociència i Nanotecnologia (ICN2), Campus de la UAB, 08193 Bellaterra, Spain
victor.puntes@icn.cat

        Prof. V. Puntes, Prof Jordi Arbiol
Institució Catalana de Recerca i Estudis Avançats (ICREA), Passeig Lluís Companys, 23, 08010 Barcelona, Spain

        Dr. R. Barrena, A. García, L. Delgado, Dr. X. Font, Dr. A. Sánchez
Department of Chemical Engineering, Escola d'Enginyeria, Universitat Autònoma de Barcelona, 08193 Bellaterra, Spain

        Dr. E. González
Instituto Geofísico, Facultad de Ingeniería, Pontificia Universidad Javeriana, 110231, Bogota, Colombia

        Prof. P. Glatzel, K. Kvashnina.
European Synchrotron Radiation Facility (ESRF), Grenoble, France

        Prof. J. Arbiol
Institut de Ciència de Materials de Barcelona, ICMAB-CSIC, Campus de la UAB, 08193 Bellaterra, Spain

Biomass transformation into biogas is a potential solution to the pressing problems to mankind of a decrease in mineral oil resources, increase in energy demand,[1] and the need to improve organic waste processing towards a sustainable scenario for waste management all over the world.[2] Additionally, increased biogas production efficiency will favor the implantation of tailored-size reactors fed with local biomass in isolated areas.[3] The process, methanogenesis, is performed by the methanogen microorganism *Archaea*, which has an important role in the carbon cycle, participating in the decay of organic matter in anaerobic ecosystems, such as sediments, marshes and sewage. Therefore, bacterial colony performance enhancement has been greatly explored,[4] including codigestion and pretreatments of the biomass, by selective hydrolysis, heating the waste,[5] or adding iron salts.[6]

For *Archaea* microorganisms, as for all forms of life, iron homeostasis is critical. In fact, Fe^{2+} and Fe^{3+} ions are essential for power generation and DNA replication, amongst other vital functions.[7] The ease with which iron ions up-take or lose electrons makes them an ideal and versatile cofactor for numerous proteins, while excess iron can easily generate highly reactive and toxic free radicals that are deleterious to different biomolecules (nucleic acids and lipids, amongst others). Although iron is one of the most abundant elements in the earth's crust, its bioavailability is not as great as one would expect since the majority is in the insoluble 3+ state. The solubility limits, at pH 7, are 0.1 M for Fe^{2+} and 10^{-18} M for Fe^{3+}.

Indeed, trace elements necessary for anaerobic digestion, as Fe^{2+}, Ni^{2+} or Ca^{2+},[6a] have been used at μM to mM concentrations.[8] Therefore, the addition of Fe^{2+} at 37°C to an anaerobic reactor in the form of chloride resulted in a modest increase (5 – 10 %) in biogas production during the first 24–48 hours. Afterwards, the gas production decreased and it was similar to that of the controls.[9] Similarly, at room temperature, iron sulfate was used, and up to 40% of increase in methane production was found (with 0.15 mg/mL) before the high concentration of iron ions started to kill bacteria, which consequently dramatically decreased biogas production,[6b] since iron, despite of being essential, at higher concentrations, is toxic.

The increase also only occurred in the first 48 hours and, once the iron salt was consumed, biogas production followed as for the controls.

Thus, we hypothesized that maintaining optimal iron concentrations in an anaerobic digester is a critical step to boost bacterial activity. For this challenging task, small iron oxide NPs, which at non-saturation conditions slowly dissolve, are good candidates to achieve such activity boosting. We introduce here a novel concept of dosing ions by size and surface-state engineering of NPs; here the NP acts as the carrier and the released ion as the active compound. Thanks to the specific lability and persistency of such NPs they can first disperse and then progressively dissolve over an extended period of time to yield the dietary supply of iron for the microorganisms in the reactor. As the NP becomes smaller, the energy needed to maintain its surface becomes increasingly important. Thus, small NPs are unstable and they can be designed to provide ions in a controlled manner via modification of their size, surface state, and concentration. It is worth noting that, in the anaerobic methanogenic conditions of the closed digester, addition of iron gives rise to insoluble precipitates of ferric hydroxide that are reduced to Fe^{2+} which is soluble and therefore becomes bioavailable.

In a typical experiment, when 100 ppm of 7 nm iron oxide NPs (Fe_3O_4) were introduced into an anaerobic waste treatment reactor, the biogas production per gram of organic matter increased by up to 180%, which is the largest improvement in methane production to date and approaches the theoretical limits of organic matter into biogas conversion (**Figure 1**).[10] The results presented correspond to the cumulative biogas production obtained. We did determine the composition of the biogas produced at different time points by gas chromatography. Results showed there is not only an enhancement of biogas produced from digesters with Fe_3O_4 NPs, but also that this is richer in CH_4 (8% more CH_4 respect controls). Concretely CH_4 percentage in the biogas is 56.6±3.1% in the case of Fe_3O_4 NPs and 48.8±0.2% in the control experiments. Less than 1% of the biogas produced is other gases as H_2S and the rest is CO_2.

3

Anaerobic assays were performed in 600 mL gas-tight reactors, equipped with a pressure transducer to monitor biogas production.[11] Each anaerobic reactor contained: 250 mL of bacterial inoculum from a local waste-management plant (Consorci per a la Defensa de la Conca del riu Besòs, Granollers, Spain), the sample (an ammonium salt as Tetramethylammonium hydroxide (TMAOH) 10 mM solution as control solvent or nanoparticle suspension), 1.7 g of cellulose, and water up to 500 mL. The pH value of each reactor was adjusted to 8 (if necessary) with citric acid, and nitrogen gas was used to purge oxygen from the system, prior to incubation at 37°C for 60 days. The 60 day process took place in a closed reactor and it could not be interrupted, as every time that the reactor is opened this allows oxygen to get in, killing a fraction of the bacterial productive substrate. Control experiments with 10 mM of TMAOH showed no biogas production enhancement (Figure 1).
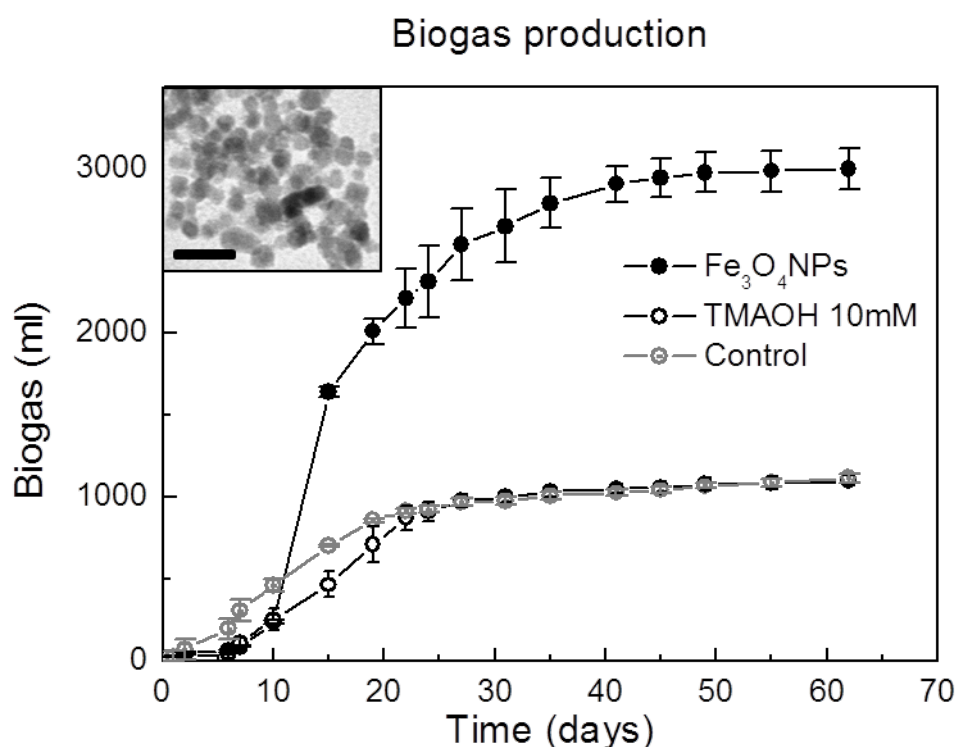

Figure 1. Biogas production boosted by the sustained release of iron ions from nanoparticles (NPs). Biogas production of the anaerobic digestion processes using 7 nm Fe_eO_eNPs (black line, solid circles), 10mM TMAOH (black line, hollow circles) and control experiment without NPs and TMAOH (grey line) is showed. Three replicate experiments

were performed for each case. Inset: Transmission electron microscopy (TEM) image of the employed 7-nm Fe_3O_4 NPs, as-synthesized (scale bar is 20 nm).

We monitored by different techniques NP modification during biogas production, within the complex medium of the digester, to observe how X-ray diffraction (XRD), X-ray absorption spectroscopy (XANES), and magnetometry NP signatures evolved (**Figure 2A-D**). As can be seen in Figure 1, the process saturates at around 40 days, with the most active time being 10 to 20 days; this time-period is where we focus our analysis. Superconducting quantum-interference device (SQUID) magnetometry indicated loss of saturation magnetization and increase of coercivity as the methane production progressed, which is consistent with NP dissolution. Thus, as the NPs become smaller, so does the saturation magnetization, and as the surface contribution increases, the coercive field, H_c, broadens. Besides, XRD showed progressively smaller and broader diffraction peaks, which also indicate decrease in both size and number of NPs: In the XRD peaks, the full width at half maximum (FWMH) is directly related to the crystal size via the Scherrer equation; the broader the peak, the smaller the diffracting crystal domain. X-ray absorption near-edge spectroscopy (XANES), which measures the electronic states of iron in the whole sample, showed an evolution of the electronic structure of the iron towards richer Fe^{3+} ion content, and a decrease of the contribution from Fe^{2+} signal, as is especially notable in the fall-off with time of the peak at 7.11 keV. Thus, this shows an increase of the Fe^{3+}/Fe^{2+} ratio with time in the digester, what initially would be surprising due to the anaerobic conditions and the high solubility of Fe^{2+} vs Fe^{3+}. In addition, Electron energy-loss spectroscopy (EELS) analysis of the Fe valence state in the NPs (**Figure 2E**) showed an evolution of the initial Fe/O ratio (from 3/4 towards 2/3), which would correspond to a progressive loss of iron ions from the NPs. The EELS spectral profile along the red arrow in figure 2E clearly shows a signal arising from Fe when crossing the NP. The relative composition of the NP is measured on the middle of the NP once the background signals arising from the electron microscopy substrate have

been removed. All in all, this is consistent with the dissolution of Fe^{2+} and its progressive metabolization to Fe^{3+}. This forces the NP dissolution while decreasing the amount of Fe^{2+} in the sample. XRD analysis further support these hypothesis: while the elemental analysis (EELS) of the observed NPs matches either with maghemite or hematite (Fe_2O_3), there is no hint of hematite from the XRD curves suggesting that the NPs are transformed from magnetite to maghemite-like nanocrystals. . Note that the maghemite (Fe_2O_3) crystalline-diffraction pattern is very close to that of the originally introduced magnetite (Fe_3O_4), especially at the nanoscale.[12]

Measurements at longer times (>40 days) show that the NPs do not completely stop evolving, especially in their magnetic behavior, however, they evolved less than they did earlier, in parallel with the methane production. This NP evolution is of particular interest to the nanotoxicology community as it suggests that NPs are less persistent and stable within the environment than they are currently believed to be.
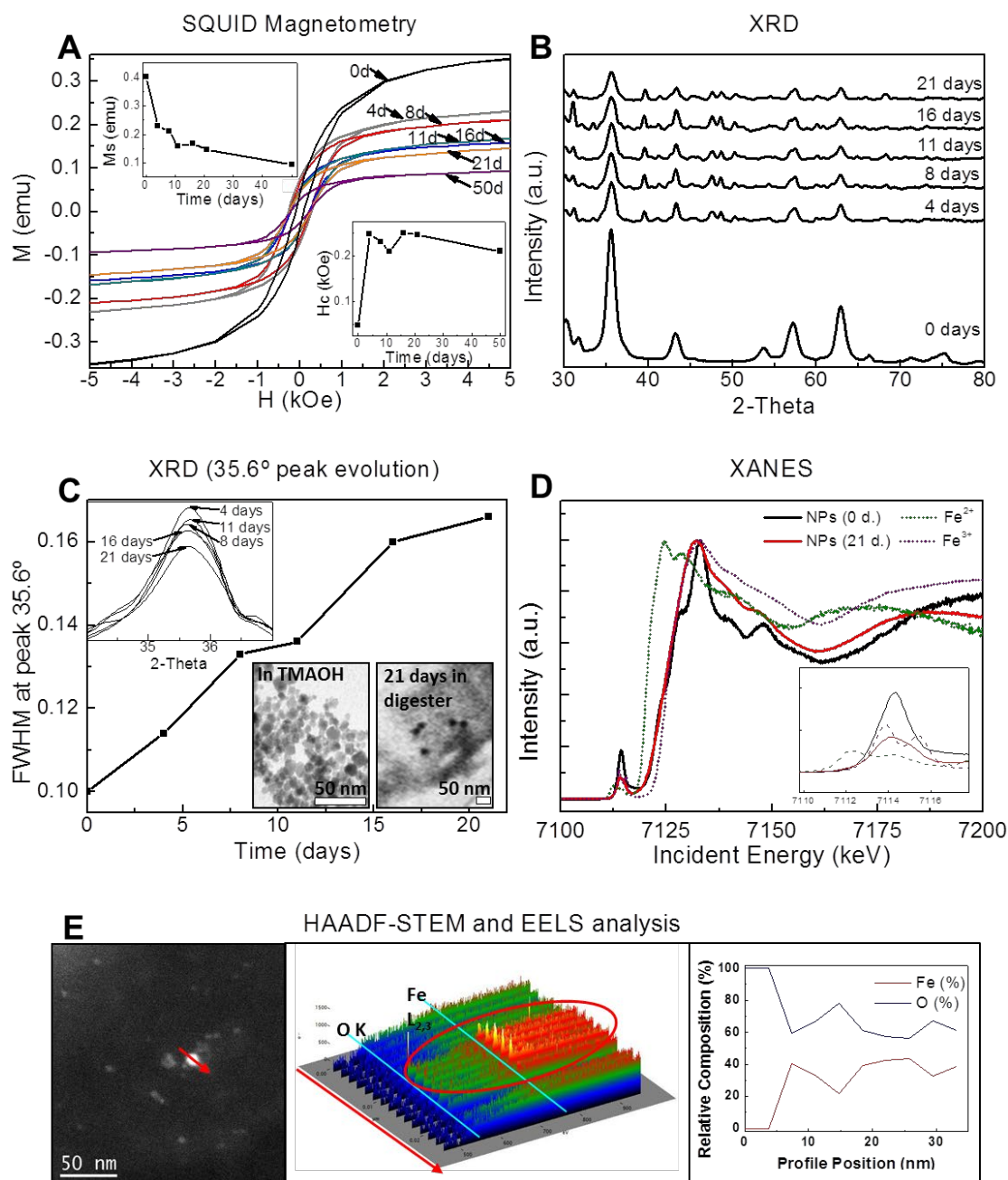
Figure 2. Fe₃O₄ NP characterization during anaerobic digestion. A) SQUID magnetometry measurements. Insets show the loss of saturation magnetization (M_s) and the increase of coercivity over time. **B)** XRD spectra of Fe₃O₄ NPs in the digester at different time points showing smaller and broader diffractions peaks over time. **C)** FWHM of the peak at 35.6 2-Θ°. FWHM increase is observed over time. **C Inset)** TEM images of Fe₃O₄ NPs as-synthesized and after 21 days in the digester. **D)** XANES spectra of Fe^{2+} (from $FeCl_2$), Fe^{3+} (from $Fe(NO_3)_3$, and Fe₃O₄ NPs at day 0 and after 21 days in the digester. Fe₃O₄ NP signatures evolve over time. Inset: peak at 7.11 KeV. **E) HAADF-scanning transmission electron microscopy (STEM) and EELS analyses of iron oxide NPs in the sludge.** Left: HAADF image of iron oxide NPs modified by microbiota metabolism. Center and right: EELS spectral profile along the red arrow, showing a clear signal due to Fe, Fe^{2+}, or Fe^{3+} when crossing the nanoparticle. The relative composition measured at the middle of the

nanoparticle once the O signal background coming from the TEM substrate surrounding the particle is removed reveals 60.5% O and 39.5% Fe.

TEM images also showed that already after 21 days there was significant modification of the size distribution (**Figure 3**), where a few large NPs, larger than the originals (25 instead of the original 7 nm average size), associated with organic matter were observed together with small NPs (which indeed are smaller than the originals, with an average size of 5 nm). This organic matter comes likely from the inoculum (as TEM controls show and does not look like cellulose) to which NPs appear strongly associated. Note that this tendency to interact with organic matter should provide a suitable iron supply at the point of need (here, the anaerobic cell), which is important since release of iron far away from where it is needed may promote deactivation of iron ions (Fe^{2+} or Fe^{3+}) by interacting with oxygen or sulfur in molecules present in the waste.
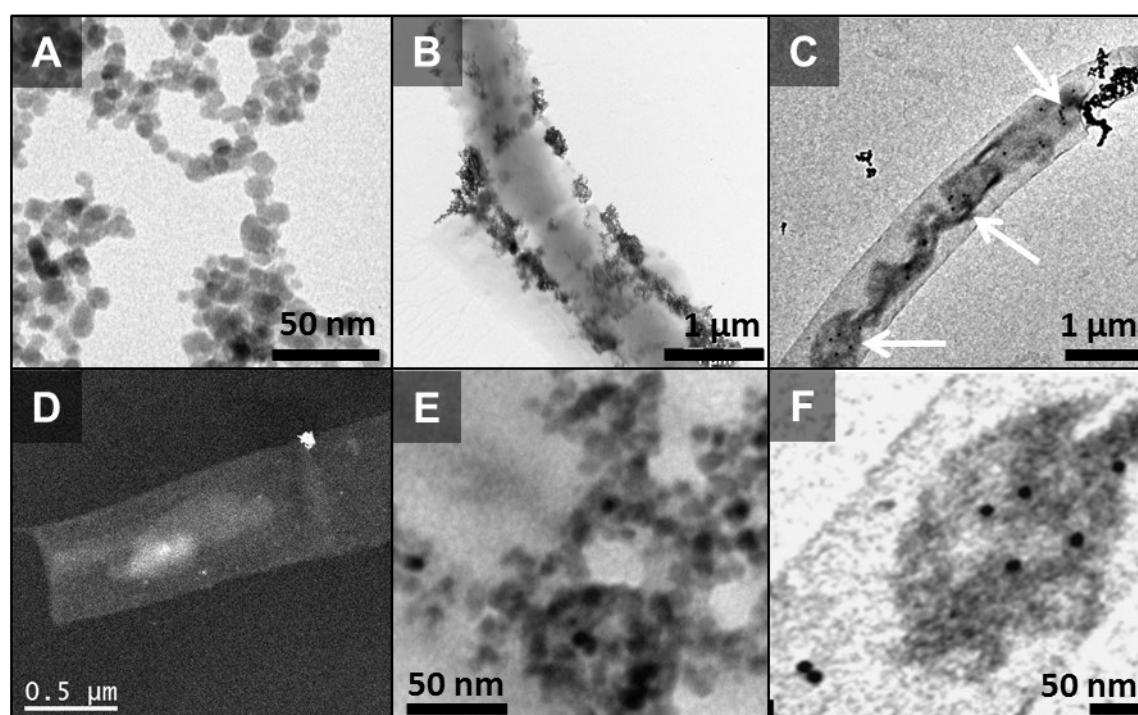

Figure 3. Fe_3O_4 NP characterization during anaerobic digestion. A) TEM image of the 7 nm Fe_3O_4 NPs as-synthesized; **B)** TEM image of the Fe_3O_4 NPs associated with the membranes of microorganisms present in the sludge taken after 21 days of incubation. **C)** TEM image also taken after 21 days of incubation; biotransformed iron is labeled with arrows. **D)** high-angle annular dark-field (HAADF) image that shows the biotransformed NPs. **E)** TEM image of the Fe_3O_4 NPs present in the sludge taken after 21 days of incubation. **F)** Enlargement of an area in image C.

The ensemble of the analytical results is consistent with the iron from the NPs being released, employed, and (at least some of it) re-mineralized into a second generation of iron NPs in a process that maintains a concentration of free iron ions over a long period of time.

A control experiment was performed dispersing the same NPs in pure water as in the digester (**Figure 4A**). In these conditions, we clearly observed a progressive NP dissolution and the consequent modification of the NP size distribution (**Figure 5**), which is strongly dependent on environmental conditions. Controlled release of an active component, iron in this case, from an aggregate is described by the Noyes-Whitney equation,[13] which relates the rate of dissolution of solids to the properties of the solid and the dissolution medium. In the case of colloidal suspensions this phenomenon is manifested in the well-known Ostwald ripening,[14] in which concentration gradients cause small precipitates to dissolve and larger ones to grow: smaller precipitates are more unstable, and additionally, larger ones display a larger surface (although a smaller surface to volume ratio) for trapping ions, leading to a broadening of the size distribution during dissolution.

If we compare the biogas production profiles in the presence and absence of NPs (Figure 1), we observe that while in the latter case, the biogas production is virtually over at day 21, the production of biogas in the presence of NPs still runs up to day 40, where all of the organic substrate is consumed. As at this point there is still a significant amount of remaining NPs in the reactor that can yield further amounts of iron; this indicates that biogas production could be further increased with the same NPs if more organic matter were supplied. It is also important to note that there is a delay in the increase of biogas production when the NPs are present. Even more, the production in the presence of NPs is lower in the first 10 days than without the NPs, likely due to colony adaptation/acclimation to the presence of the NPs. However, the dissolution of iron is observed from the very first day, which suggests that

there is a threshold iron dose, around a few milligrams per liter, which results in the rapid increase of methane production.

In a dose-response experiment, one can observe how, in the working conditions, biogas production increases with NP concentration, peaks at 0.27 mg/mL, and then decreases, likely due to an excess of reactive iron ions and the consequent lethal effects on the methane-producing bacteria (**Figure 4B**). To control dose one can also control size and surface coating, since they have direct effects on dissolution rate, which is size- and environment-dependent. Thus, when we tested the NP dissolution in different atmospheres, different dissolution rates were observed, with open air resulting in the fastest rate and an N_2 atmosphere in the slowest. Interestingly, dissolution in the reactive environment of the digester was faster than in N_2, although both are anoxic, indicating the importance of Archaea metabolism in iron oxide NPs transformation.

We also compared different stabilizers, such as organic salts and proteins, which can act as ion scavengers (**Figure 4C**), and in these cases no difference was found in the total production of biogas. It has been explained that a critical NP size and stability is needed for dissolution in the time frame of anaerobic digestion processes. And as discussed, surface state also affects NP solubility. It is well known that Fe_3O_4 NPs develop persistent (hard) protein corona while TMAOH is easily removed from the NP surface when more affinity ligands, as proteins, are present in solution.[15] We observed that in the experimental conditions, the coating of the NP surface with serum proteins is not enough to prevent iron oxide particles dissolution and the biological effect due to iron ions released is also observed for coated NPs. Probably the NP coating is also detached or processed, so that any difference is only found at short times, where a further delay in production is observed (serum proteins at the NP surface could act as ion scavengers as they interact with Fe ions), but later the process catches up.
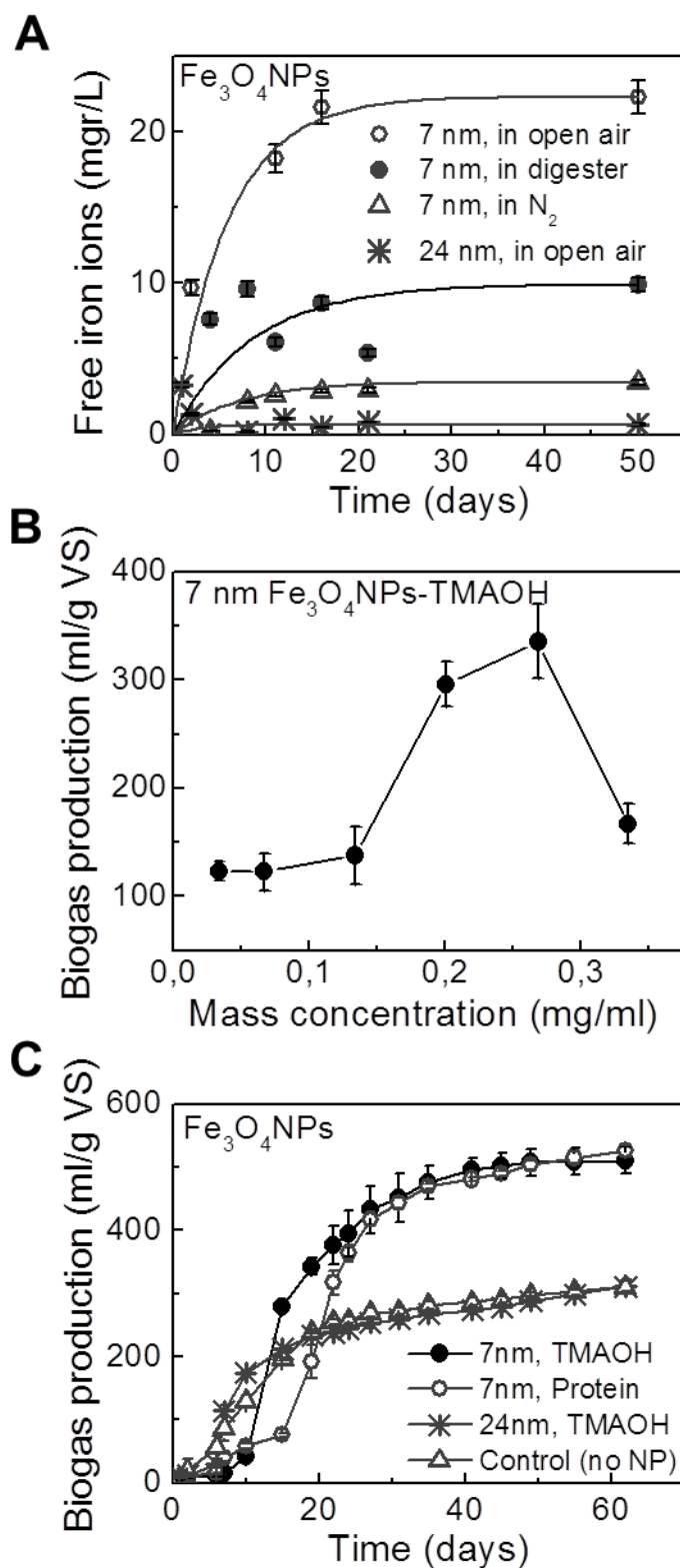
Figure 4. Biogas production boosted by the sustained release of Fe²⁺ from NPs. A) Release of iron ions from Fe_3O_4 NPs in different media. **B)** Dose-response of biogas production at different NP concentrations. **C)** Biogas production of the anaerobic digestion processes using different types of Fe_3O_4 NPs.
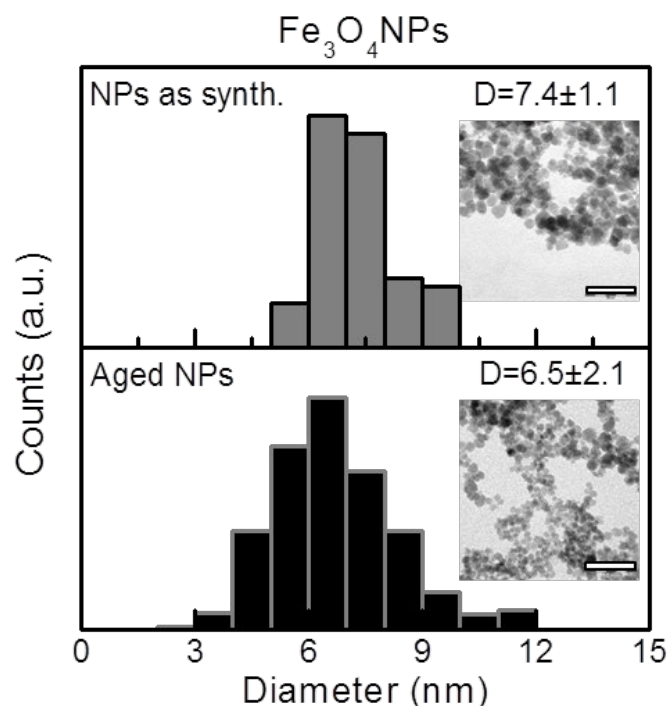
Figure 5. Size distribution of Fe₃O₄ NPs as synthesized and aged. Up: Size distribution of NPs after synthesis: mean diameter=7.4±1.1; **Down:** Size distribution of aged NPs in biological media (after 2 days): mean diameter=6.5±2.1. **Insets:** TEM images where scale bar is 50 nm.

The driving force behind NP dissolution mainly depends on the solubility of the constituent ions in a given environment and the concentration gradient of NPs in solution.[16] In these cases, the interfacial free energy is always a positive term and acts to destabilize the NPs. As a consequence, at very small sizes when many ions reside at the surface, the NPs are unstable; such NPs will dissolve rather than grow. This phenomenon is referred to as the Gibbs-Thomson effect where precipitates dissolve or grow due to concentration gradients of reacting species. Thus, small NPs are close to the critical radius, which strongly depends on the monomer saturation and the NPs environment. When this environment is changed, then, the NP may enter into a critical zone where it became unstable and dissolves. For a given mass, the kinetics of dissolution will be proportional to the specific surface area and the coordination of the atoms at that surface. In fact, in a standard face-centered cubic (fcc) crystal lattice, as in the present case, the coordination number is 12 and for surfaces 9, this can

be decreased by reducing size, in the small NPs, down to 7.[17] Furthermore, the surface tension[18] and activation energy relevant to dissolution[19] are also size-dependent for small NPs. Indeed, it has been reported that generally, below 20-30 nm, changes in the crystal structure and crystal (surface) defects enhance NP dissolution.[19-20] This fact is consistent with our observations that 7-nm NPs dissolve at an appropriate rate to maintain the necessary supply of iron at the milligram per liter concentration, in the experimental conditions, while 24-nm NPs do not dissolve observably in the experimental time.

Dissolution is a process in which mass transfers from the solid surface to the liquid phase. After this, the solute ions must migrate through the boundary layers surrounding the surface of the crystal to the bulk of the solution. This step involves the transfer of the ions away from the solid-liquid interface into the bulk of the liquid phase by diffusion or convection. If the released ions are used up in competing reactions, their mobility is high and their concentration low, so the system is moved far away from the saturation point; *sink* conditions are reached and the NPs tend towards complete dissolution. If during dissolution the concentration of available ions returns the system to saturation, the ions will dissolve more slowly or not at all.

Thus, to attain good control of biomass processing, NPs can be used as unique ion dispensers. In the case of the anaerobic waste digester this fact boosts biogas production. The dose of active iron that the bacteria will be exposed to is determined by the NP size, surface state, and concentration: larger NPs may release iron too much, too slowly, while the smaller ones may release it too little, too quickly. This observation of iron supply and remineralization recalls the role of the ferritin protein, responsible for maintaining iron homeostasis within the body by mineralizing/dissolving iron. This work is also extremely inspiring for dosing drugs with nanocarriers to cells of selected organs. In this way nanoiron behaves in analogy to drug delivery systems, in which the particle contains and protects a reservoir of active species, the ion, which is transported and released near the biological target

sites. Needless to say, colloidal stability is critical in these experiments (hence the need for stabilizers) since the aggregation of NPs will lead to larger entities which dissolve much more slowly.

In summary, production of methane by conversion of biomass is an important source of fuel that will help to overcome challenges of energy shortage. Addition of Fe^{2+} ions to an anaerobic bacterial reactor can increase methane production, however introducing such ions can give rise to toxicity and excess reactivity. Here we show that iron oxide nanoparticles (NPs) act as a unique Fe^{2+} source because of their lability, denseness, and large size, especially in the anaerobic methanogenic conditions of the reactor. Since small NPs are unstable, they can be designed to provide ions in a controlled manner. The evolution of the NPs during operation has been followed by an array of spectroscopic techniques, and we obtain the highest ever reported improvement of methane production.

Experimental Section.

Chemicals. Iron (II) chloride (FeCl$_2$, 98%), iron (III) chloride (FeCl$_3$, ≥98%), Tetramethylammonium Hydroxide (TMAOH, 1.0M in H$_2$O), Sodium Hydroxide (NaOH, ≥98%), Potassium hydroxide (KOH, ≥85%), Potassium chloride (KCl, ≥99%) and foetal bovine serum (FBS) were purchased from Sigma-Aldrich and used as received.

Synthesis of Nanoparticles. Fe$_3$O$_4$ NPs used were synthesized in the aqueous phase, using milli-Q grade water. All reagents were purchased from Sigma-Aldrich and used as received. All the synthesis procedures are based in preexisted ones available in the scientific literature with modifications to be adapted to large-scale yields.

a) Tetramethylammonium hydroxide (TMAOH) stabilized, 7 nm mean diameter Fe$_3$O$_4$ NPs. Based on Massart's method[21] amounts of 1 mmol FeCl$_2$ and 2 mmol FeCl$_3$ were dissolved in 50 mL deoxygenated water and then added dropwise to 50 mL of a solution of deoxygenated TMAOH 1M. After 30 min of vigorous stirring under a N$_2$ stream, the Fe$_3$O$_4$ precipitate was washed by soft magnetic decantation and redissolved in TMAOH 1mM to obtain the final stable colloidal solution of Fe$_3$O$_4$ NPs.

b) TMAOH stabilized, 20 nm mean diameter Fe$_3$O$_4$ NPs. Massart method was also employed, adapting the procedure described in Nyiro-Kosa et al.[22] Amounts of 3.4 mmol FeCl$_2$ and 4.2 mmol FeCl$_3$ were dissolved in 50 ml of a solution of NaOH 1M. After 30 min of vigorous stirring under a N$_2$ stream, washing steps and resuspension in TMAOH as previously described were followed to obtain the final stable colloidal solution of Fe$_3$O$_4$ NPs.

c) Protein coated, 7 nm mean diameter Fe$_3$O$_4$ NPs. FBS and Fe$_3$O$_4$ NPs synthesized as described in *a)* were mixed at 1:10 (v/v) and left 7 days at RT. In these conditions, serum proteins coated all NP surface.[15]

d) TMAOH stabilized, 5 nm mean diameter γ-Fe₂O₃NPs. Based on Lu et al.[23] amounts of 0.675 g $FeCl_3$, 0.25 g $FeCl_2$ and 2 g KCl were ground in a mortar for 30 min at RT. After, 0.61 g KOH was added and the mixture grinded 30 min more at RT. The final mixture was dispersed in milli-Q water, washed three times and finally redispersed in TMAOH 1mM.

Instrumentation.

Transmission electron microscopy (TEM) images were acquired with a JEOL 1010 electron microscope operated at low accelerating voltage (80 kV) to increase contrast.

High resolution TEM (HRTEM) analysis was performed on a JEOL 2100 with an accelerating voltage of 200 kV equipped with an energy-dispersive X-ray spectroscopy (EDX) detector. Samples for TEM and HRTEM were prepared by drop casting onto carbon-coated TEM grids. The grids were left to dry at room temperature. Observations were made on different parts of the grid and with different magnifications. More than 500 particles were computer-analyzed and measured to calculate size distributions.

X-ray diffraction (XRD) data were collected on a PANalytical X´Pert diffractometer using a Cu Kα radiation source (λ=1.541 Å). In a typical experiment, the 2θ diffraction (Bragg) angles were measured by scanning the goniometer from 25° to 90°. The samples were prepared by centrifugation of the sludge containing the NPs at 40.000 g to precipitate the NPs. The supernatant was discarded and samples were dried at room temperature to avoid further NP transformations. Peak positions and their full width at half maximum (FWHM) were determined using the X´Pert HighScore program after baseline correction.

Induced coupled plasma-mass spectroscopy (ICP-MS) was performed using an ICP-MS Agilent instrument (Model: 7500cx) with a detection limit of 0.02386 ppb. For ICP-MS analysis the samples were dissolved in concentrated aqua regia, which was then heated to ensure complete dissolution of all the metals, and diluted to an optimal concentration for ICP-

MS analysis. Ga was used as the internal standard and the integration time/point and time/mass were 0.1 sec and 0.3 sec, respectively with a 3x repetition. The samples for ICP-MS measurements were prepared by two steps of centrifugation. First, the sludge containing the NPs was centrifuged at 40.000 g for 45 min. Supernatant was recovered and washed again by centrifugation at the same conditions. This last supernatant, where free ion ions remain, was kept for ICP-MS analysis. To ensure the efficient separation of free ions from the particles, dialysis of this last supernatant and further ICP-MS analysis of the fraction inside and outside the membrane is carried out. As iron concentration is the same in both fractions, this proves that there are no NP left in the supernatant"

Magnetization measurements were performed on a superconducting quantum-interference device (SQUID) magnetometer (MPMS Quantum Design). The hysteresis cycles were obtained at 10 K in a magnetic field varying from +5 to −5 kOe. The sample preparation was performed by dispersing the particles in paraffin to have a solid dispersion of noninteracting NPs, which was introduced then into gelatin capsules under ambient conditions.

X-Ray Absorption Near Edge Spectroscopy (XANES) measurements were performed at beamline ID26 of the European Synchrotron Radiation Facility (ESRF) in Grenoble/France.[24] The incident energy was selected using the <311> reflection from a double Si crystal monochromator. Rejection of higher harmonics was achieved by three Si mirrors working under total reflection. The incident photon flux was monitored by detecting the X-rays scattered from a foil using a photodiode. Four spherically bent (R=1m) Ge crystal analyzers in <440> reflection were chosen suitable for the detection of the $K\alpha 1$ emission line of Fe (6405 eV). The combined energy bandwidth was 0.9 eV. Sample, analyzer crystal and photon detector (avalanche photodiode) were arranged in a vertical Rowland geometry. The high energy resolution fluorescence detected (HERFD)-XANES spectra were recorded at scattering angles covering 72 - 99 degrees in the horizontal plane. Fluorescence detected XANES data are affected by incident beam self absorption.[25] A reliable correction for self

absorption could not be achieved and the spectral intensities are therefore distorted. The conclusions drawn in this work are not affected by this experimental artefact.

Biogas determination:

Anaerobic sludge: Sludge for inoculation of anaerobic experiments was obtained from mesophilic anaerobic reactors in real wastewater treatment plants in the province of Barcelona. Sludge was obtained from the recirculation of these reactors. This sludge was maintained under starving conditions during two weeks at 37°C to remove any biodegradable organic matter that could interfere in further results.[26]

Main substrate: As sole substrate for anaerobic digestion crystalline cellulose (Panreac, Barcelona, Spain) was used as described in Barrena et al.[11]

Procedure: The test methodology to determine the anaerobic biogas production was adapted from the German standard DIN-38414. Anaerobic assays were performed in 600 ml gas tight reactors, equipped with a pressure transducer to monitor biogas production.[27] Each anaerobic reactor contained: 250 ml of inoculum, 250 ml of sample (solvent or nanoparticles suspension), 1.7 g of cellulose and water to 500 ml. pH of each reactor was adjusted to 8 (if necessary) and nitrogen gas was used to purge oxygen previous to incubation to 37ºC during 21 days. Reactors were manually stirred and biogas was purged every workday. A blank and a reference test were also performed. The blank test (250 ml of inoculum and water to 500 ml) was performed to subtract biogas production from any biodegradable organic matter contained in the inoculum. The control test (250 ml of inoculum, 1.7 g of microcrystalline cellulose and water to 500 ml) was performed to compare biogas production with sample tests. Each experiment was carried out in three independent triplicate experiments. The results are shown as the average value from nine experiments with the corresponding standard deviation.

Biogas composition determination:

Methane and carbon dioxide content in the biogas were analyzed by means of a Hewlett Packard Chromatograph (HP 5890) equipped with a thermal conductivity detector (TCD) and a Supelco Porapack Q (250 °C) 3 m × 1/8" column. Helium was the carrier gas at 338 kPa, and the oven, injector and detector temperatures were 70, 150 and 180 °C, respectively. A total sample volume of 100 μL was used for chromatography.

References.

[1]   a) A. Jess, *Energ Policy* **2010**, *38*, 4663; b) C. Wolfram, O. Shelef, P. Gertler, *J Econ Perspect* **2012**, *26*, 119.

[2]   a) A. Distaso, *International Journal of Sustainable Development* **2012**, *15*, 220; b) D. Y. Hou, A. Al-Tabbaa, P. Guthrie, K. Watanabe, *Environ Sci Technol* **2012**, *46*, 2494.

[3]   A. D. Karve, *Science* **2003**, *302*, 987.

[4]   a) M. Morita, K. Sasaki, *Appl Microbiol Biot* **2012**, *94*, 575; b) I. M. Nasir, T. I. M. Ghazi, R. Omar, *Appl Microbiol Biot* **2012**, *95*, 321; c) Yadvika, Santosh, T. R. Sreekrishnan, S. Kohli, V. Rana, *Bioresource Technol* **2004**, *95*, 1.

[5]   a) J. Abelleira, S. I. Perez-Elvira, J. R. Portela, J. Sanchez-Oneto, E. Nebot, *Environ Sci Technol* **2012**, *46*, 6158; b) C. Bougrier, J. P. Delgenes, H. Carrere, *Biochem Eng J* **2007**, *34*, 20.

[6]   a) D. J. Hoban, L. Vandenberg, *Journal of Applied Bacteriology* **1979**, *47*, 153; b) P. P. Rao, G. Seenayya, *World Journal of Microbiology & Biotechnology* **1994**, *10*, 211.

[7]   J. F. Banfield, H. Z. Zhang, *Rev Mineral Geochem* **2001**, *44*, 1.

[8]   L. Vandenberg, K. A. Lamb, W. D. Murray, D. W. Armstrong, *Journal of Applied Bacteriology* **1980**, *48*, 437.

[9]   M. S. Ram, L. Singh, M. V. S. Suryanarayana, S. I. Alam, *Water Air and Soil Pollution* **2000**, *117*, 305.

[10]   a) A. Donoso-Bravo, F. Mairet, *J Chem Technol Biot* **2012**, *87*, 1375; b) H. B. Nielsen, I. Angelidaki, *Water Sci Technol* **2008**, *58*, 1521.

[11]   R. Barrena, E. Casals, J. Colon, X. Font, A. Sanchez, V. Puntes, *Chemosphere* **2009**, *75*, 850.

[12]   A. Corrias, G. Mountjoy, D. Loche, V. Puntes, A. Falqui, M. Zanella, W. J. Parak, M. F. Casula, *J Phys Chem C* **2009**, *113*, 18667.

[13]   M. S. Sherrill, *Science* **1936**, *84*, 217.

[14]   a) W. Ostwald, *Lehrbuch der Allgemeinen Chemie.* (W. Engelmann, Leipzig, Germany, 1896), vol. 2, part 1; b) W. Ostwald, *Zeitschrift für physikalische Chemie* **1897**, *22*, 289.

[15]   E. Casals, T. Pfaller, A. Duschl, G. J. Oostingh, V. Puntes, *Small* **2011**, *7*, 3479.

[16]   P. Borm, F. C. Klaessig, T. D. Landry, B. Moudgil, J. Pauluhn, K. Thomas, R. Trottier, S. Wood, *Toxicological Sciences* **2006**, *90*, 23.

[17]   a) M. Bowker, *Nat Mater* **2002**, *1*, 205; b) C. T. Campbell, S. C. Parker, D. E. Starr, *Science* **2002**, *298*, 811.

[18]   A. N. Goldstein, C. M. Echer, A. P. Alivisatos, *Science* **1992**, *256*, 1425.

[19]   D. V. Talapin, A. L. Rogach, M. Haase, H. Weller, *Journal of Physical Chemistry B* **2001**, *105*, 12278.

[20]   a) C. F. Fan, J. Chen, Y. Chen, J. F. Ji, H. H. Teng, *Geochimica Et Cosmochimica Acta* **2006**, *70*, 3820; b) A. L. Rogach, D. V. Talapin, E. V. Shevchenko, A. Kornowski, M. Haase, H. Weller, *Advanced Functional Materials* **2002**, *12*, 653.

[21]   a) R. Massart, *Ieee Transactions on Magnetics* **1981**, *17*, 1247; b) J. P. Jolivet, R. Massart, J. M. Fruchart, *Nouv J Chim* **1983**, *7*, 325.

[22]   I. Nyiro-Kosa, D. C. Nagy, M. Posfai, *Eur J Mineral* **2009**, *21*, 293.

[23]   J. Lu, S. H. Yang, K. M. Ng, C. H. Su, C. S. Yeh, Y. N. Wu, D. B. Shieh,

        Nanotechnology **2006**, *17*, 5812.

[24]   C. Gauthier, V. A. Sole, R. Signorato, J. Goulon, E. Moguiline, *J Synchrotron Radiat*

        1999, *6*, 164.

[25]   M. Bianchini, P. Glatzel, *J Synchrotron Radiat* **2012**, *19*, 911.

[26]   A. Schievano, M. Pognani, G. D'Imporzano, F. Adani, *Bioresource Technol* **2008**, *99*,

        8112.

[27]   S. Ponsa, I. Ferrer, F. Vazquez, X. Font, *Water Res* **2008**, *42*, 3972.

Figures and figure captions.

Figure 1.
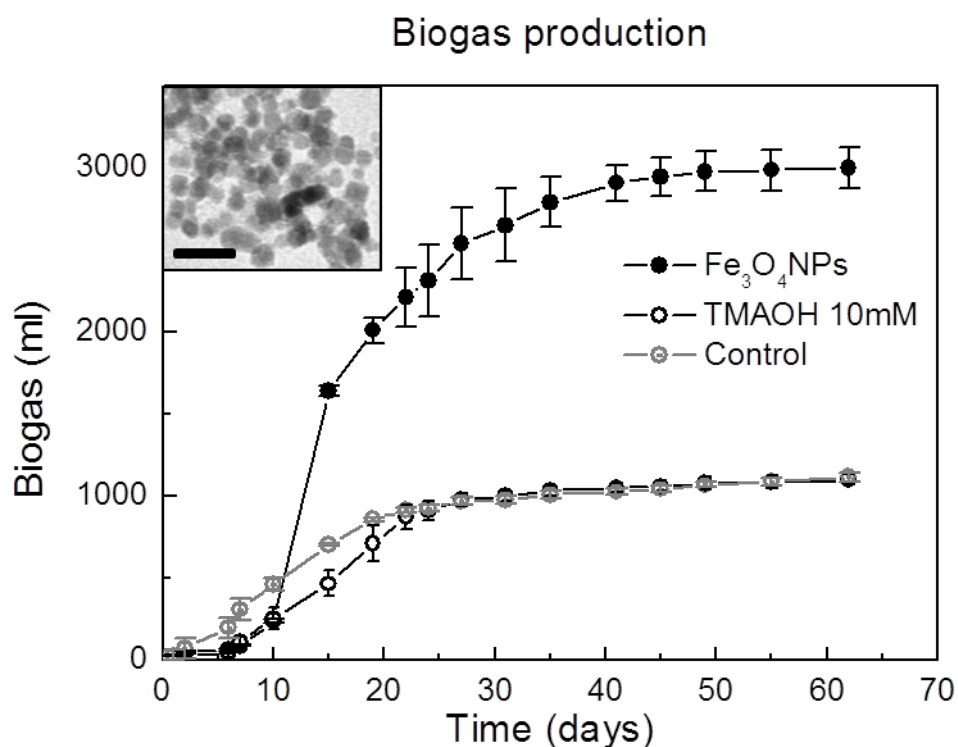
Figure 1. Biogas production boosted by the sustained release of iron ions from nanoparticles (NPs). Biogas production of the anaerobic digestion processes using 7 nm Fe_eO_eNPs (black line, solid circles), 10mM TMAOH (black line, hollow circles) and control experiment without NPs and TMAOH (grey line) is showed. Three replicate experiments were performed for each case. Inset: Transmission electron microscopy (TEM) image of the employed 7-nm Fe_3O_4 NPs, as-synthesized (scale bar is 20 nm).

Figure 2.

Figure 2. Fe₃O₄ NP characterization during anaerobic digestion. A) SQUID magnetometry measurements. Insets show the loss of saturation magnetization (M_s) and the increase of coercivity over time. **B)** XRD spectra of Fe₃O₄ NPs in the digester at different time points showing smaller and broader diffractions peaks over time. **C)** FWHM of the peak at 35.6 2-Θ°. FWHM increase is observed over time. **C Inset)** TEM images of Fe₃O₄ NPs as-synthesized and after 21 days in the digester. **D)** XANES spectra of Fe^{2+} (from $FeCl_2$), Fe^{3+} (from $Fe(NO_3)_3$, and Fe₃O₄ NPs at day 0 and after 21 days in the digester. Fe₃O₄ NP signatures evolve over time. Inset: peak at 7.11 KeV. **E) HAADF-scanning transmission electron microscopy (STEM) and EELS analyses of iron oxide NPs in the sludge.** Left: HAADF image of iron oxide NPs modified by microbiota metabolism. Center and right: EELS spectral profile along the red arrow, showing a clear signal due to Fe, Fe^{2+}, or Fe^{3+} when crossing the nanoparticle. The relative composition measured at the middle of the nanoparticle once the O signal background coming from the TEM substrate surrounding the particle is removed reveals 60.5% O and 39.5% Fe.
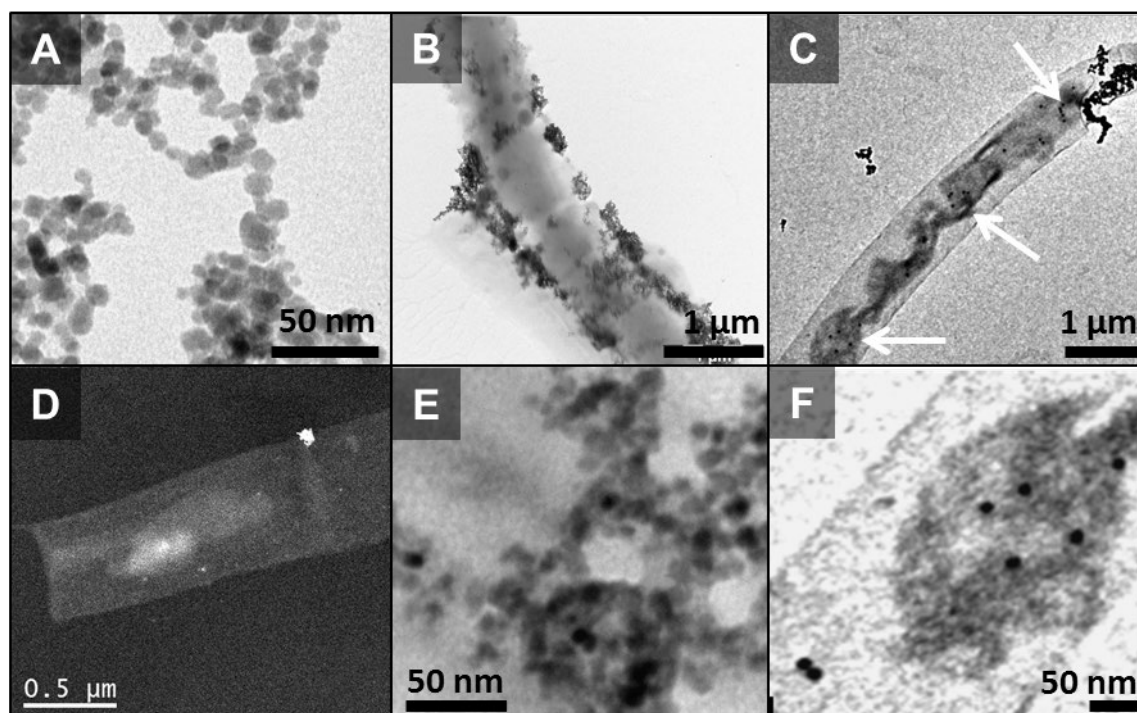
Figure 3

Figure 3. Fe₃O₄NP characterization during anaerobic digestion. A) TEM image of the 7 nm Fe_3O_4 NPs as-synthesized; **B)** TEM image of the Fe_3O_4 NPs associated with the membranes of microorganisms present in the sludge taken after 21 days of incubation. **C)** TEM image also taken after 21 days of incubation; biotransformed iron is labeled with arrows. **D)** high-angle annular dark-field (HAADF) image that shows the biotransformed NPs. **E)** TEM image of the Fe_3O_4 NPs present in the sludge taken after 21 days of incubation. **F)** Enlargement of an area in image C.
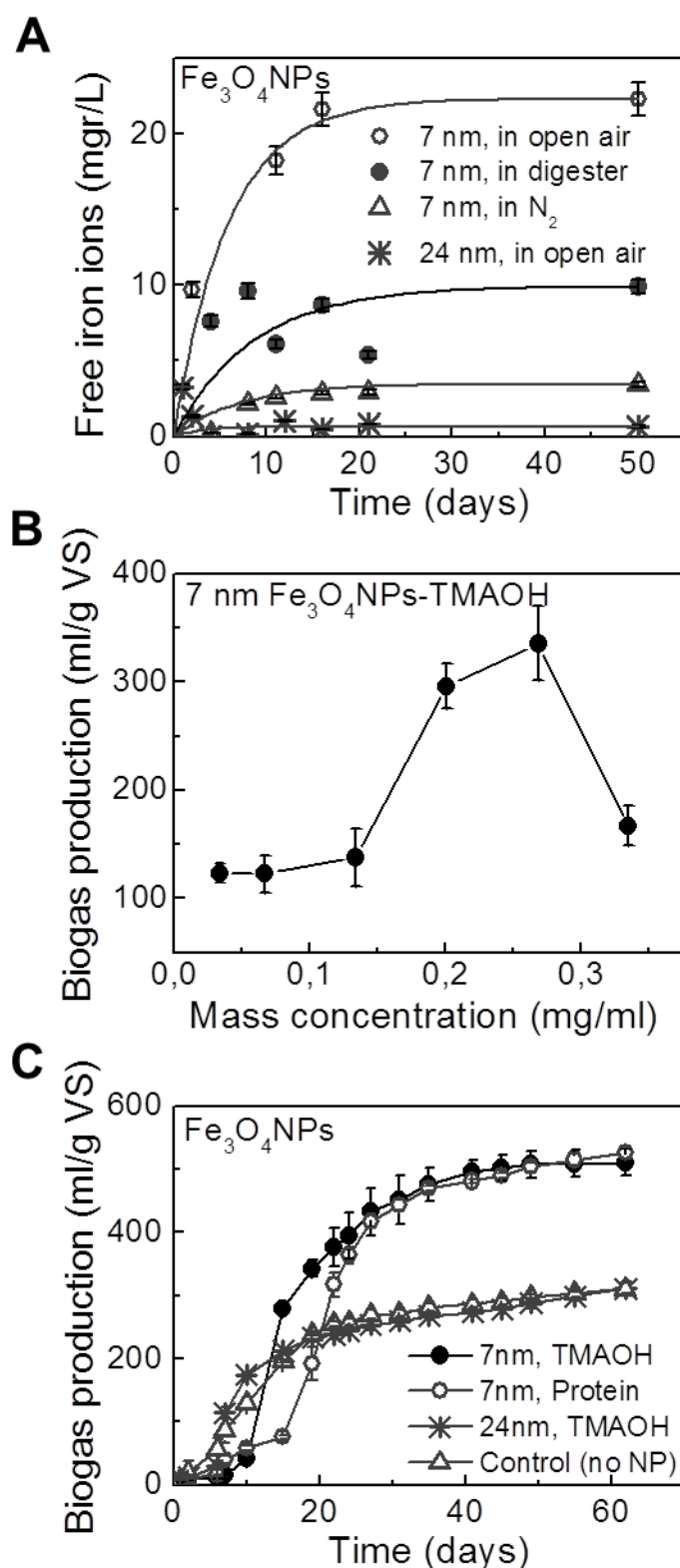
Figure 4.

Figure 4. Biogas production boosted by the sustained release of Fe²⁺ from NPs. A) Release of iron ions from Fe_3O_4 NPs in different media. **B)** Dose-response of biogas production at different NP concentrations. **C)** Biogas production of the anaerobic digestion processes using different types of Fe_3O_4 NPs.
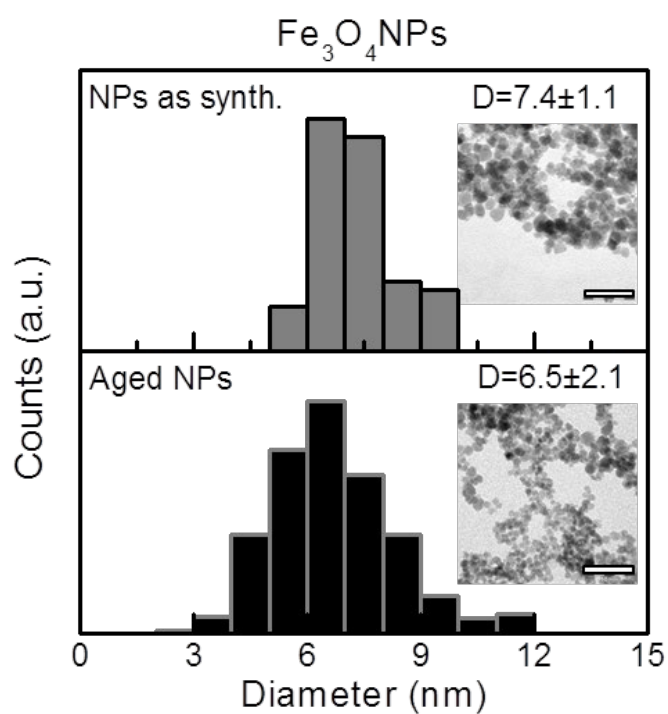
Figure 5.

Figure 5. Size distribution of Fe₃O₄ NPs as synthesized and aged. Up: Size distribution of NPs after synthesis: mean diameter=7.4±1.1; **Down:** Size distribution of aged NPs in biological media (after 2 days): mean diameter=6.5±2.1. **Insets:** TEM images where scale bar is 50 nm.

The table of contents entry should be 50−60 words long, and the first phrase should be bold. The entry should be written in the present tense and impersonal style.

A novel concept of dosing iron ions using Fe_3O_4 engineered nanoparticles is used to improve biogas production in anaerobic digestion processes. Since small NPs are unstable, they can be designed to provide ions in a controlled manner, and the highest ever reported improvement of methane production is obtained. The nanoparticles evolution during operation is followed by an array of spectroscopic techniques.

(TOC Keyword)

iron oxide nanoparticles, nanoparticles dissolution, nanoparticles evolution, anaerobic digestion, biogas production.
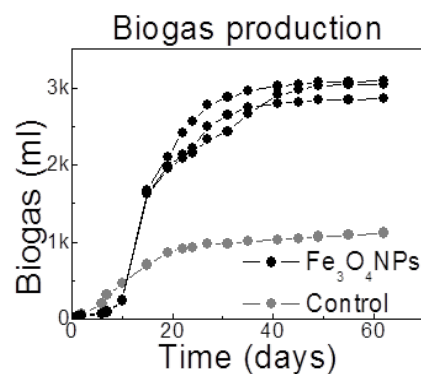
(Authors)

Eudald Casals, Raquel Barrena, Ana García, Edgar González, Lucía Delgado, Xavier Font, Jordi Arbiol, Pieter Glatzel, Kristina Kvashnina, Antoni Sánchez, and Víctor Puntes*

(Title)

Programmed Iron Oxide Nanoparticles Disintegration in Anaerobic Digesters Boosts Methane Production.

(ToC figure ((size: 55 mm broad × 50 mm)))

Supporting Information

Programmed Iron Oxide Nanoparticles Disintegration in Anaerobic Digesters Boosts Methane Production.

Eudald Casals, Raquel Barrena, Ana García, Edgar González, Lucía Delgado, Xavier Font, Jordi Arbiol, Pieter Glatzel, Kristina Kvashnina, Antoni Sánchez, and Víctor Puntes*

Figure S1. TEM images of the time evolution of Fe$_3$O$_4$ NPs in the anaerobic reactor.
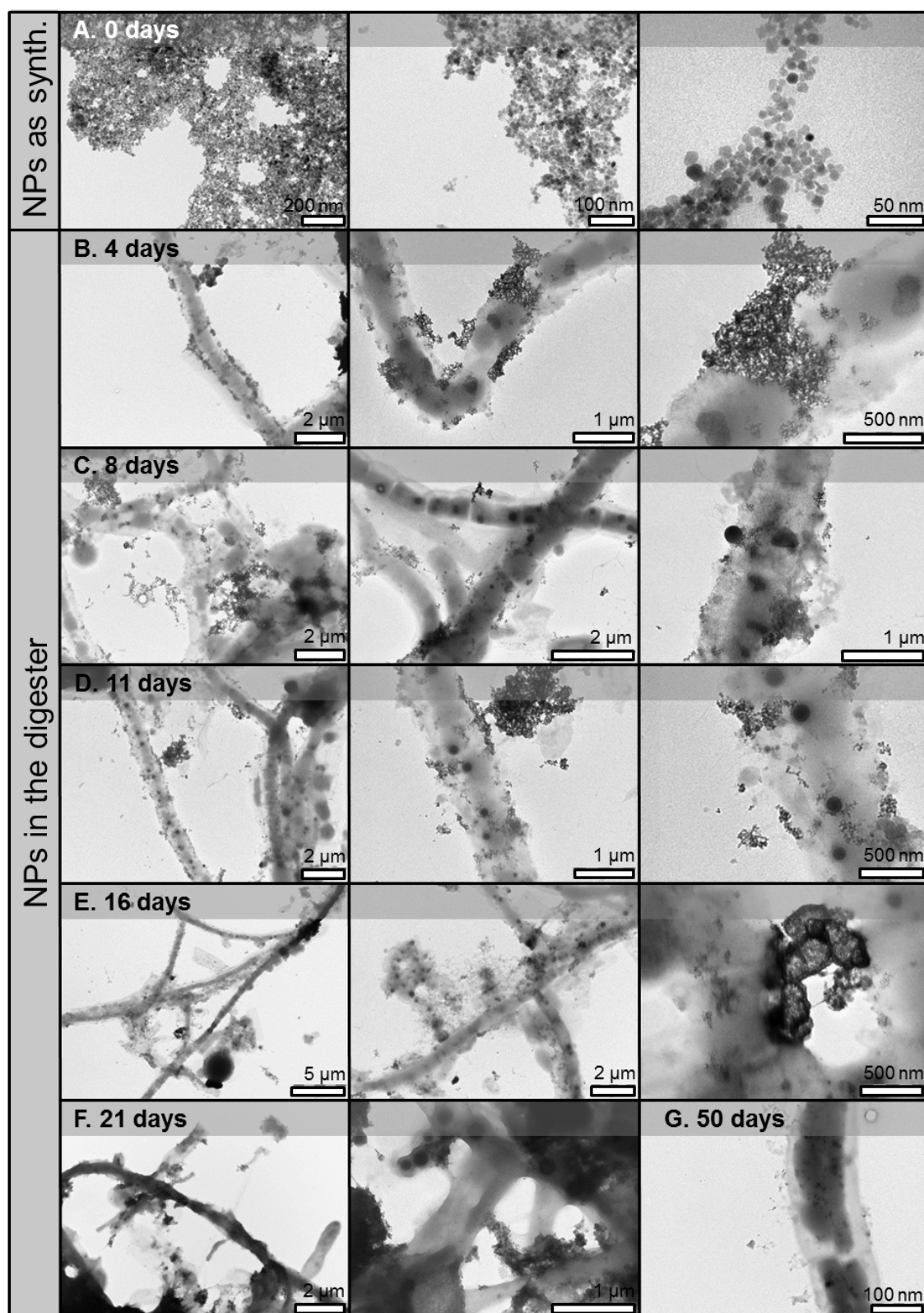

Figure S1. TEM images of the time evolution of Fe$_3$O$_4$ NPs in the digester. A) NPs as synthesized. B-G) NPs after 4, 8, 11, 16, 21 and 50 days in the anaerobic reactor.

Table S1.

Incubation Time	FWMH (35.6° peak)	Hc (Oe)	Ms (emu)
0 days	0.101	47	0.403
4 days	0.114	248	0.231
8 days	0.133	231	0.212
11 days	0.136	210	0.159
16 days	0.160	250	0.168
21 days	0.166	247	0.146
50 days		211	0.093

Table S1. *Values of the increase of full width at half maximum (FWHM) at the 35.6° peak, increase of Coercivity (Hc) and decrease of Saturation Magnetization (Ms).*